Dalton Transactions

ROYAL SOCIETY OF CHEMISTRY

PAPER

View Article Online
View Journal | View Issue

Cite this: *Dalton Trans.*, 2023, **52**, 15101

An ethynyl-modified interpenetrated metal–organic framework for highly efficient selective gas adsorption†

Xueyue Yu,[a] Ziyang Huang,[b] Rajamani Krishna,[c] Xiaolong Luo *[a,b] and Yunling Liu *[a]

Received 31st August 2023,
Accepted 29th September 2023

DOI: 10.1039/d3dt02834h

rsc.li/dalton

An ethynyl-modified interpenetrated MOF material with *lvt* topology, $[Cu_2(BTEB)(NMF)_2]\cdot NMF\cdot 8H_2O$ (compound **1**, H_4BTEB = 4,4′,4″,4‴-(benzene-1,2,4,5-tetrayltetrakis(ethyne-2,1-diyl))tetrabenzoic acid, NMF = *N*-Methylformamide), was successfully synthesized by using an alkynyl-functionalized H_4BTEB organic ligand under solvothermal conditions. Structural analysis shows that compound **1**, consisting of a tetradentate carboxylic acid ligand and classical $[Cu_2(CO_2)_4]$ paddle-wheel structure building units, has a rare 4-connected *lvt* topology with dual interpenetrating structure, which can improve the framework stability, as well as the gas adsorption capacity and selectivity due to the restricted pore channel. According to the study of gas adsorption performance, compound **1** with a larger surface area, boasts a superior adsorption capacity for small gas molecules. Also, ideal adsorption solution theory (IAST) computational simulation shows that compound **1** has good gas adsorption selectivity for C_3H_8/CH_4, indicating its potential application in gas separation.

Introduction

In recent years, the continuous emission of greenhouse gases resulted in an imbalance of energy absorption and emission. The accumulation of energy in the atmosphere can lead to global warming and severe environmental and ecological problems. The greenhouse effect is mainly caused by the excessive burning of coal and oil in modern industries.[1–5] Using organic amines for carbon dioxide fixation requires advanced production equipment and high costs for adsorbent regeneration.[6] An efficient, cheap and renewable material is needed to capture CO_2.

Methane is a primary component of natural gas, coalbed methane, biogas, and an essential energy source.[7–11] However, the obtained raw natural gas is always accompanied by various impurities, such as carbon dioxide, ethane, and propane.[12–15] The presence of impurity gases reduces the energy conversion rate of natural gas, and the acidic carbon dioxide also poses a severe pipeline corrosion hazard during natural gas transportation.[16,17] Therefore, there is an urgent need to develop a material with excellent selective adsorption and separation properties to purify natural gas.

In the past two decades, porous MOFs materials, as a new type of advanced functional materials, have shown extensive applications in the fields of host–guest chemistry,[18–20] nonlinear optics,[21–23] catalysis,[24–27] magnetism,[28–30] gas storage and separation[31–39] due to their structural features such as high surface area, large pore volume, high density of open metal sites (OMSs), abundant Lewis base sites (LBSs), and the capability of functionalization and post-modification synthesis. Gas storage and separation is one of the most extensive research areas for MOFs materials, truly maximizing the advantages of pore structure design and reflecting the irreplaceable role of other inorganic materials. In addition, the topology or pores of MOFs can be well controlled by adjusting different metal ions and organic ligands with different structures and functional groups. The ordered pore structure, high porosity, and surface area all create the conditions for storing and separating gases.

When organic ligands containing functional groups such as alkenyl, alkynyl, or azo groups are introduced into MOFs materials, it is possible to expand the extended ligands and thus expand the structure of MOFs to increase their porosity

[a]*State Key Laboratory of Inorganic Synthesis & Preparative Chemistry, Jilin University, Changchun 130012, P. R. China. E-mail: yunling@jlu.edu.cn; Fax: +86 431 85168624*
[b]*School of Chemistry and Life Science, Advanced Institute of Materials Science, Changchun University of Technology, Changchun, 130012, PR China*
[c]*Van 't Hoff Institute for Molecular Sciences, University of Amsterdam, Science Park 904, 1098 XH Amsterdam, The Netherlands. E-mail: r.krishna@contact.uva.nl*

†Electronic supplementary information (ESI) available: Structure information, XRD, TGA, isosteric heat of CO_2, CH_4, C_2H_6, C_3H_8. C_2H_4 and C_2H_2. Crystal data and structure refinement. CCDC 2018785. For ESI and crystallographic data in CIF or other electronic format see DOI: https://doi.org/10.1039/d3dt02834h

without changing the symmetry of the original ligands themselves.[40–44] However, with the increasing size of organic ligands, MOFs' porosity grows surprisingly while their structures' stability gradually decreases.[45] Therefore, researchers have turned their attention to interpenetrating structures, some of which were found to increase the stability of the framework and the surface area of MOFs.[46–48]

Based on the above view, we successfully prepared a Cu-MOF material with a dual interpenetrating skeleton structure using a solvothermal synthesis method $[Cu_2(BTEB)(NMF)_2]\cdot NMF\cdot 8H_2O$ (compound **1**). Compound **1** has a rare *lvt* topological structure composed of an alkynyl-functionalized organic ligand and classical $[Cu_2(CO_2)_4]$ structure building units. The structural interpenetration enabled compound **1** with a high surface area and low porosity. As expected, compound **1** exhibits commendable separation effects on C_2H_2/CO_2 (4.2) and C_3H_8/CH_4 (204.7) at 298 K, suggesting the potential applications in gas adsorption and separation.

Experimental

Materials and methods

The chemicals and reagents for this study were purchased from commercial sources and used without further purification. Powder X-ray diffraction (PXRD) data were collected on a Rigaku D/max 2550 diffractometer with Cu-Kα radiation (λ = 1.5418 Å) over the 2θ range of 4–40° at room temperature. Thermogravimetric analyses (TGA) were performed using a TA Q500 thermogravimetric analyzer with a heating rate of 10 °C min^{-1} up to 800 °C in air. Elemental analyses (C, H, N and O) were performed with a vario MICRO elemental analyzer.

Synthesis of compound 1

The H_4BTEB organic ligand was synthesized according to the previous literature.[49] CuI (5 mg, 0.026 mmol) and H_4BTEB (4 mg, 0.007 mmol) were dissolved in 1 mL of NMF in a 20 mL glass vial and sonicated for 5 min. Then, 0.02 mL HNO_3 (2.2 mL HNO_3 in 10 mL NMF) was added into the mixture and heated at 85 °C for 24 h. Green block single crystals were obtained, washed with NMF, and dried in air (65% yield based on CuI). Elemental analysis (wt%) for compound **1**: calculated: C, 61.62; H, 3.12; N, 3.12, found: C, 61.09; H, 5.197; N, 3.95.

X-ray crystallography

Crystallographic data for compound **1** was collected on a Bruker Apex II CCD diffractometer using graphite-monochromated Mo-K_α (λ = 0.71073 Å) radiation at temperature 273 K. The structure of compound **1** was solved by direct methods and refined by full-matrix least-squares on F^2 using SHELEX-2014/7.[50] All the metal atoms were located first, and then the oxygen, carbon, and nitrogen atoms of compound **1** were subsequently found in difference Fourier maps. The hydrogen atoms of the ligand were placed geometrically. All non-hydrogen atoms were refined anisotropically. There were lots of disordered solvent molecules in the cavity of the structure, the PLATON/SQUEEZE was applied to remove their diffraction contribution.[51] Topology analysis for compound **1** was obtained by using ToposPro.[52] Crystallographic data for compound **1** (2018785†) have been deposited with Cambridge Crystallographic Data Centre. The summary of the crystallographic data and related parameters can be seen in Table S1,† while the selective bond lengths and angles of these compounds are given in Table S2.†

Gas adsorption measurements

All gas adsorption measurements (N_2, CO_2, CH_4, C_2H_6, C_3H_8, C_2H_4 and C_2H_2) were performed on Micromeritics instruments (Models ASAP 2420 and ASAP 2020). Before gas adsorption measurements, compound **1** was exchanged with methanol for 3 days to completely remove the guest NMF and water molecules. Samples were activated by drying under a dynamic vacuum at 60 °C for 1 hour. Prior to obtained gas measurements, samples were dried again using the 'outgas' function of the surface area analyzer for 10 h at 150 °C.

Results and discussion

Crystal structure of compound 1

Crystallized in the orthorhombic crystal system, *Cmca* space group, compound **1** contains two secondary building units. The classical $[Cu_2(CO_2)_4]$ paddle-wheel is the inorganic secondary structural motif connected to four organic ligands. The 4-linked alkynyl functionalized carboxylic acid ligand constitutes the organic secondary structural motif, both of which can be simplified to quadrilateral shapes, interconnected to form a three-dimensional skeletal structure with a dual interpenetration and a *lvt* topology with the point symbol $[4^2\cdot 8^4]$ (Fig. 1a–d, Fig. S1†). Compound **1** has a pore channel of about 5.4 Å × 5.4 Å along the [001] direction (van der Waals radius removed). The total solvent-accessible volume of compound **1** was estimated to be 68.5% by using PLATON (Fig. 1e).

Although the structure of compound **1** is similar to that of BUT-43,[49] there are many differences between them. The terminal groups of the metal clusters in compound **1** are coordinated to NMF, whereas BUT-43 is coordinated to water molecules. The different coordination environments lead to the crystallisation of the two compounds in different space groups. And the different ligand's bending degrees (177.5° for BUT-43 and 155.5° for compound **1**, respectively) and the benzene ring's rotation angles (13.6°, 27.3°, 32.4°, 34.7° for BUT-43 and 24.1°, 57.0° for compound **1**, respectively) led to different degrees of interpenetration (Fig. S2†), resulting in the differences of their single-cell parameters (Table S3† and Fig. 2). The structural variations make the gas adsorption and selectivity properties of compound **1** different from those of BUT-43 (Table 1). The two compounds have similar pore volumes of 68.5% and 71.3%, respectively. The BET surface area of compound **1** is 899 $m^2\ g^{-1}$, which is lower than the 1124 $m^2\ g^{-1}$ of BUT-43. Although the gas adsorption capacity

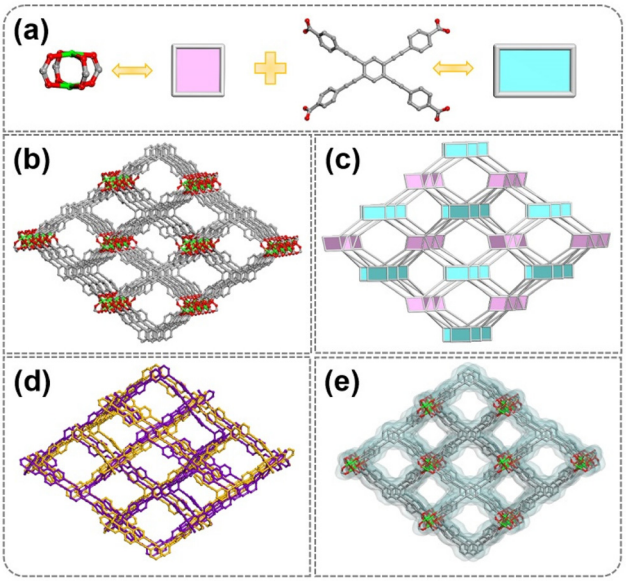

Fig. 1 Description of the structures of compound **1**: (a) Cu paddlewheel SBUs, and organic $BTEB^{4-}$ ligand viewed as 4-c nodes; (b) ball and stick model of compound **1**; (c) polyhedral view of the *lvt* topology; (d) two-fold interpenetrated framework of compound **1**; (e) connolly surface view of compound **1**. Color scheme: carbon = gray, oxygen = red, copper = green. Guest molecules and H atoms have been omitted for clarity.

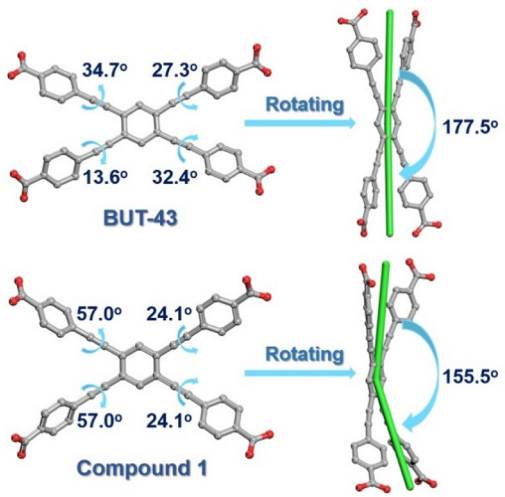

Fig. 2 The difference of ligand's bending degrees and the benzene ring's rotation angles.

of compound **1** was lower than that of BUT-43, the separation capacity of C_2H_2/CH_4 was slightly higher than that of BUT-43.

PXRD and thermogravimetric analysis

As shown in Fig. S3,† the diffraction peak positions of PXRD patterns are the same between the experimentally measured and the simulated one, proving that the experimentally synthesized compound **1** is a pure phase. The activated compound **1** maintains high crystallinity, indicating that the skeleton of the material did not collapse after removing guest molecules. The results of thermogravimetric analysis of compound **1** are shown in Fig. S5.† Compound **1** loses about 17% of its weight before 150 °C, which can be attributed to removing the guest NMF and H_2O molecules from the pore channels. The structure of compound **1** can be stabilized until about 300 °C and loses about 62% of its weight after 300 °C due to the decomposition of organic ligands, implying that the structure of compound **1** starts to collapse, ultimately resulting in the formation of metal oxide CuO. After activation with ethanol, the sample had almost no weight loss until 300 °C, indicating that the guest molecules NMF and H_2O in the pore channels were almost completely removed after the solvent exchange of compound **1**.

Table 1 Comparison of the gas adsorption and selectivity properties for compound **1** and BUT-43

			Compound **1**	BUT-43
Total solvent-accessible volume			68.5%	71.3%
N_2 (77 K)	BET surface area ($m^2\ g^{-1}$)		899	1124
	Langmuir surface area ($m^2\ g^{-1}$)		1219	—
Adsorption capacities ($cm^3\ g^{-1}$)	C_2H_2	273 K	60.8	85.6
		298 K	55.6	67.7
	CO_2	273 K	48.3	51.3
		298 K	29.5	42.9
	CH_4	273 K	18.5	16.3
		298 K	11.3	12.7
Selectivity (0.5 : 0.5)	C_2H_2/CH_4		14.3	8.4
	C_2H_2/CO_2		4.2	35.2

Gas adsorption and separation behaviors

The porosity of compound **1** was investigated using N_2 adsorption under 77 K conditions. As shown in Fig. S6,† the maximum adsorption of N_2 by compound **1** was 351 $cm^3\ g^{-1}$, the calculated BET surface area was 899 $m^2\ g^{-1}$, and the Langmuir surface area was 1219 $m^2\ g^{-1}$. The results indicate that compound **1** has permanent porosity and is a typical microporous material with potential applications in small molecular gas adsorption.

The adsorption capacity of compound **1** for carbon dioxide is 48.3 and 29.5 $cm^3\ g^{-1}$ at 273 and 298 K under standard atmospheric pressure, comparable to some reported MOFs.[53,54] The experimental results suggest compound **1** will be an advanced material for storing carbon dioxide gas. Furthermore, in order to investigate the adsorption capacity of compound **1** for small light hydrocarbon gases and the subsequent theoretical calculation of gas adsorption separation, we tested small gases such as CH_4, C_2H_6, C_3H_8, C_2H_4, and C_2H_2.

The maximum adsorption capacities of compound **1** were 18.5 and 11.3 $cm^3\ g^{-1}$ for CH_4, 63.3 and 52.6 $cm^3\ g^{-1}$ for C_2H_6, 60.8 and 56.3 $cm^3\ g^{-1}$ for C_3H_8, 56.6 and 47.0 $cm^3\ g^{-1}$ for C_2H_4, and 60.8 and 55.6 $cm^3\ g^{-1}$ for C_2H_2, respectively at 273

and 298 K understand standard air pressure, as shown in Fig. 3. In addition, to evaluate the interaction between gas molecules and the host skeletons, the isosteric heats of adsorption (Q_{st}) for CO_2, CH_4, C_2H_6, C_3H_8, C_2H_4, and C_2H_2 in compound **1** were calculated based on the pure component isotherms at 273 and 298 K. The calculated Q_{st} values are 22, 15, 27, 38, 27, and 27 kJ mol^{-1}, respectively (Fig. S7 and S8†).

IAST uses experimentally obtained gas adsorption isotherm curves to predict the separation performance of two-component mixed gases. After fitting the dual-site Langmuir–Freundlich (DSLF) for the single-component gas adsorption of CO_2, CH_4, C_2H_6, C_3H_8, C_2H_4, and C_2H_2 measured in the experiment at 298 K, the selective separation of two-component gas mixtures with different ratios was calculated by using the IAST method. The carbon dioxide and methane gas mixture ratios are 50% : 50% and 5% : 95%. At 298 K and 760 mmHg, the separation ratio of compound **1** is 3.2 for a mixture of equimolar CO_2/CH_4 and 3.1 for a mixture of CO_2/CH_4 with a molar ratio of 5% : 95% (Fig. 4a and b). The theoretical simulation results show that compound **1** has a higher separation ability for the mixture of carbon dioxide and methane than Cu-MOF[55] and some other materials.[56,57] As shown in Fig. 4, under the conditions of 298 K and 760 mmHg, the separation ratios of the mixture of equimolar C_2H_2/CO_2, C_2H_2/CH_4, C_2H_4/CH_4, C_2H_6/CH_4, and C_3H_8/CH_4 of compound **1** are 4.2, 14.3, 17.3, 25.5, and 204.7, respectively (Fig. 4c–d and Fig. S9†). Under the same conditions, the separation ability of compound **1** for the C_3H_8/CH_4 mixture is higher than the reported NUM-18a.[58] To further demonstrate the separation potential of compound **1**, we performed transient breakthrough simulations using the simulation methodology described in the literature.[59–65] The results indicated that compound **1** was effective in separating equimolar 2-component light hydrocarbon mixtures in a fixed bed at a total pressure of 100 kPa and a temperature of 298 K (Fig. 4e–f and Fig. S10†).

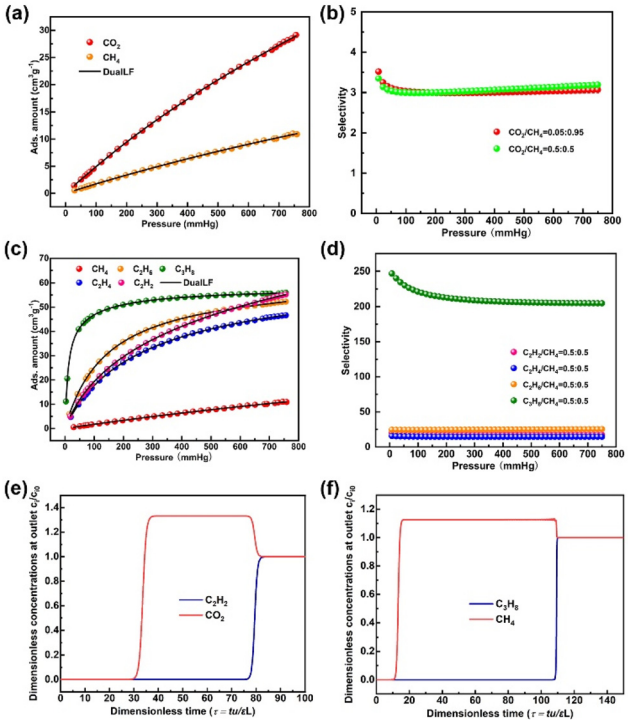

Fig. 4 CO_2, CH_4, C_2H_6, C_3H_8, C_2H_4 and C_2H_2 adsorption isotherms at 298 K along with the DSLF fits (a and c); gas mixture adsorption selectivity is predicted by IAST at 298 K and 760 mmHg for compound **1** (b and d); transient breakthrough simulations for separation of 50/50 C_2H_2/CO_2 and 50/50 C_3H_8/CH_4 (e and f) mixtures containing.

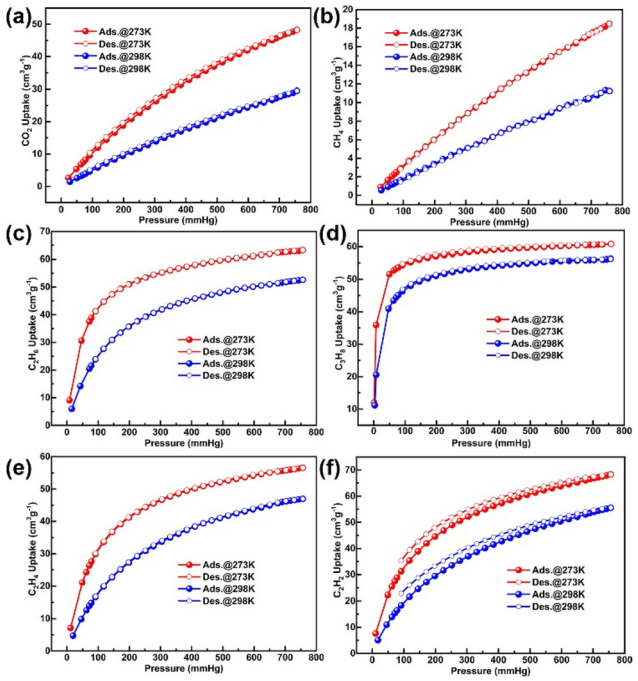

Fig. 3 (a) CO_2; (b) CH_4; (c) C_2H_6; (d) C_3H_8; (e) C_2H_4; (f) C_2H_2 gas adsorption/desorption isotherms for compound **1** at 273 and 298 K under 1 atm.

Conclusions

In summary, we successfully synthesized a Cu-MOF material with 2-fold interpenetrating *lvt* net, by utilizing alkyne-functionalized tetracarboxylic acid as the organic ligand and cuprous iodide as the metal source under solvothermal conditions. The as-synthesized MOF material possesses good adsorption capacity for various gases and exhibits excellent separation performance for methane due to the open metal sites, carbon–carbon triple bonds, and multidimensional pore system in its backbone, which shows that compound **1** has potential application value in gas separation.

Author contributions

Xueyue Yu: Conceptualization; data curation; formal analysis. Ziyang Huang: Conceptualization; data curation. Rajamani Krishna: Theoretical calculations. Xiaolong Luo:

Conceptualization; data curation; formal analysis; writing – original draft. Yunling Liu: Conceptualization; supervision; validation; writing – review & editing.

Conflicts of interest

There are no conflicts to declare.

Acknowledgements

This work was supported by the National Natural Science Foundation of China (21901021 and 22171100), the Science Research Foundation of Jilin Province (YDZJ202301ZYTS478) and China Postdoctoral Science Foundation (2021T140256).

References

1 L.-C. Lin, A. H. Berger, R. L. Martin, J. Kim, J. A. Swisher, K. Jariwala, C. H. Rycroft, A. S. Bhown, M. W. Deem, M. Haranczyk and B. Smit, *Nat. Mater.*, 2012, **11**, 633–641.
2 D. Yancy-Caballero, K. T. Leperi, B. J. Bucior, R. K. Richardson, T. Islamoglu, O. K. Farha, F. You and R. Q. Snurr, *Mol. Syst. Des. Eng.*, 2020, **5**, 1205–1218.
3 R. Custelcean, *Chem. Sci.*, 2021, **12**, 12518–12528.
4 H. Li, W. Xu, J. Qian and T.-T. Li, *Chem. Commun.*, 2021, **57**, 6987–6990.
5 C. Han, X. Zhang, S. Huang, Y. Hu, Z. Yang, T.-T. Li, Q. Li and J. Qian, *Adv. Sci.*, 2023, **10**, 2300797.
6 H. K. Knuutila, R. Rennemo and A. F. Ciftja, *Green Energy Environ.*, 2019, **4**, 439–452.
7 K. V. Kumar, K. Preuss, M.-M. Titirici and F. Rodríguez-Reinoso, *Chem. Rev.*, 2017, **117**, 1796–1825.
8 H. Li, L. Li, R.-B. Lin, W. Zhou, Z. Zhang, S. Xiang and B. Chen, *EnergyChem*, 2019, **1**, 100006.
9 R. Sahoo and M. C. Das, *Coord. Chem. Rev.*, 2021, **442**, 213998.
10 L. Li, L. Yang, J. Wang, Z. Zhang, Q. Yang, Y. Yang, Q. Ren and Z. Bao, *AIChE J.*, 2018, **64**, 3681–3689.
11 T. Wang, E. Lin, Y.-L. Peng, Y. Chen, P. Cheng and Z. Zhang, *Coord. Chem. Rev.*, 2020, **423**, 213998.
12 H. Wang, Y. Liu and J. Li, *Adv. Mater.*, 2020, **32**, 2002603.
13 L. Meng, Z. Niu, C. Liang, X. Dong, K. Liu, G. Li, C. Li, Y. Han, Z. Shi and S. Feng, *Chem. – Eur. J.*, 2018, **24**, 13181–13187.
14 R.-G. Lin, L. Li, R.-B. Lin, H. Arman and B. Chen, *CrystEngComm*, 2017, **19**, 6896–6901.
15 W.-G. Cui, T.-L. Hu and X.-H. Bu, *Adv. Mater.*, 2020, **32**, 1806445.
16 S. Zhang, M. K. Taylor, L. Jiang, H. Ren and G. Zhu, *Chem. – Eur. J.*, 2020, **26**, 3205–3221.
17 Y. Wang, S. B. Peh and D. Zhao, *Small*, 2019, **15**, 1900058.
18 M. Tu, H. Reinsch, S. Rodriguez-Hermida, R. Verbeke, T. Stassin, W. Egger, M. Dickmann, B. Dieu, J. Hofkens, I. F. J. Vankelecom, N. Stock and R. Ameloot, *Angew. Chem., Int. Ed.*, 2019, **58**, 2423–2427.
19 G. Radha, T. Leelasree, D. Muthukumar, R. S. Pillai and H. Aggarwal, *New J. Chem.*, 2021, **45**, 12931–12937.
20 J. Luo, X. Jia and C. Ren, *Matter*, 2022, **5**, 772–774.
21 Y. Ding, Y. Lu, K. Yu, S. Wang, D. Zhao and B. Chen, *Adv. Opt. Mater.*, 2021, **9**, 2100945.
22 W. P. Lustig, S. Mukherjee, N. D. Rudd, A. V. Desai, J. Li and S. K. Ghosh, *Chem. Soc. Rev.*, 2017, **46**, 3242–3285.
23 X. Wang, Y. Wang, Y. Wang, H. Liu, Y. Zhang, W. Liu, X. Wang and S. Wang, *Chem. Commun.*, 2020, **56**, 233–236.
24 M. Ding and H.-L. Jiang, *ACS Catal.*, 2018, **8**, 3194–3201.
25 Y. Han, M. A. Sinnwell, R. G. Surbella III, W. Xue, H. Huang, J. Zheng, B. Peng, G. Verma, Y. Yang, L. Liu, S. Ma and P. K. Thallapally, *Chem. Mater.*, 2020, **32**, 5192–5199.
26 M. Y. Masoomi, S. Beheshti and A. Morsali, *J. Mater. Chem. A*, 2014, **2**, 16863–16866.
27 Z. Niu, W. D. C. Bhagya Gunatilleke, Q. Sun, P. C. Lan, J. Perman, J.-G. Ma, Y. Cheng, B. Aguila and S. Ma, *Chem*, 2018, **4**, 2587–2599.
28 Y. Chen, Y. Chen, H.-C. Yi, H.-W. Gu, X.-L. Yin, D. L. Xiang and P. Zou, *Microchem. J.*, 2023, **190**, 108681.
29 M. Wakizaka, R. Ishikawa, H. Tanaka, S. Gupta, S. Takaishi and M. Yamashita, *Small*, 2023, 2301966.
30 N. Bagheri, H. A. J. Al Lawati, J. Hassanzadeh and I. Al Lawati, *Talanta*, 2023, **256**, 124272.
31 M. Feng, Y. Hu, P. Zhou, X. Wang, Y. He, X. Wang and D. Wang, *Chem. Eng. J.*, 2023, **451**, 138431.
32 Z. Chen, P. Li, R. Anderson, X. Wang, X. Zhang, L. Robison, L. R. Redfern, S. Moribe, T. Islamoglu, D. A. Gomez-Gualdron, T. Yildirim, J. F. Stoddart and O. K. Farha, *Science*, 2020, **368**, 297–303.
33 H. Wang, Z. Shi, J. Yang, T. Sun, B. Rungtaweevoranit, H. Lyu, Y.-B. Zhang and O. M. Yaghi, *Angew. Chem., Int. Ed.*, 2021, **60**, 3417–3421.
34 M. Feng, P. Zhou, J. Wang, X. Wang, D. Wang and C. Li, *Inorg. Chem.*, 2022, **61**, 11057–11065.
35 O. T. Qazvini, R. Babarao, Z.-L. Shi, Y.-B. Zhang and S. G. Telfer, *J. Am. Chem. Soc.*, 2019, **141**, 5014–5020.
36 W. Fan, X. Wang, X. Zhang, X. Liu, Y. Wang, Z. Kang, F. Dai, B. Xu, R. Wang and D. Sun, *ACS Cent. Sci.*, 2019, **5**, 1261–1268.
37 Y. Wang, M. Fu, S. Zhou, H. Liu, X. Wang, W. Fan, Z. Liu, Z. Wang, D. Li, H. Hao, X. Lu, S. Hu and D. Sun, *Chem*, 2022, **8**, 3263–3274.
38 W. Fan, S. Yuan, W. Wang, L. Feng, X. Liu, X. Zhang, X. Wang, Z. Kang, F. Dai, D. Yuan, D. Sun and H.-C. Zhou, *J. Am. Chem. Soc.*, 2020, **142**, 8728–8737.
39 W. Fan, Y. Ying, S. B. Peh, H. Yuan, Z. Yang, Y. D. Yuan, D. Shi, X. Yu, C. Kang and D. Zhao, *J. Am. Chem. Soc.*, 2021, **143**, 17716–17723.
40 X.-W. Gu, J.-X. Wang, E. Wu, H. Wu, W. Zhou, G. Qian, B. Chen and B. Li, *J. Am. Chem. Soc.*, 2022, **144**, 2614–2623.
41 X.-X. Zhang, X.-Z. Guo, S.-S. Chen, H.-W. Kang, Y. Zhao, J.-X. Gao, G.-Z. Xiong and L. Hou, *Chem. Eng. J.*, 2023, **466**, 143170.

42 Z. Di, C. Liu, J. Pang, C. Chen, F. Hu, D. Yuan, M. Wu and M. Hong, *Angew. Chem., Int. Ed.*, 2021, **60**, 10828–10832.
43 L. Zou, X. Sun, J. Yuan, G. Li and Y. Liu, *Inorg. Chem.*, 2018, **57**, 10679–10684.
44 T. M. M. Ntep, H. Breitzke, L. Schmolke, C. Schluesener, B. Moll, S. Millan, N. Tannert, I. El Aita, G. Buntkowsky and C. Janiak, *Chem. Mater.*, 2019, **31**, 8629–8638.
45 S. B. Kalidindi, S. Nayak, M. E. Briggs, S. Jansat, A. P. Katsoulidis, G. J. Miller, J. E. Warren, D. Antypov, F. Corà, B. Slater, M. R. Prestly, C. Martí-Gastaldo and M. J. Rosseinsky, *Angew. Chem., Int. Ed.*, 2015, **54**, 221–226.
46 H.-L. Jiang, T. A. Makal and H.-C. Zhou, *Coord. Chem. Rev.*, 2013, **257**, 2232–2249.
47 J. Li, J. Gu, L. Zhang and Y. Liu, *Dalton Trans.*, 2019, **48**, 5511–5514.
48 A. Ferguson, L. Liu, S. J. Tapperwijn, D. Perl, F.-X. Coudert, S. Van Cleuvenbergen, T. Verbiest, M. A. van der Veen and S. G. Telfer, *Nat. Chem.*, 2016, **8**, 250–257.
49 X.-J. Kong, Y.-Z. Zhang, T. He, X.-Q. Wu, M.-M. Xu, S.-N. Wang, L.-H. Xie and J.-R. Li, *CrystEngComm*, 2018, **20**, 6018–6025.
50 G. Sheldrick, *Acta Crystallogr., Sect. C: Struct. Chem.*, 2015, **71**, 3–8.
51 A. L. Spek, *Acta Crystallogr., Sect. C: Struct. Chem.*, 2015, **71**, 9–18.
52 V. A. Blatov, A. P. Shevchenko and D. M. Proserpio, *Cryst. Growth Des.*, 2014, **14**, 3576–3586.
53 Y. Liu, Z. Zhao, Y. Zhang, L. Zhou, X. Qin, Z. Zhao, H. Ji and K. Chai, *Microporous Mesoporous Mater.*, 2023, **354**, 112530.
54 Y. Shi, Y. Xie, H. Cui, Y. Ye, H. Wu, W. Zhou, H. Arman, R.-B. Lin and B. Chen, *Adv. Mater.*, 2021, **33**, 2105880.
55 K. N. Landström, A. Nambi, A. Kaiser and F. Akhtar, *RSC Adv.*, 2023, **13**, 16039–16046.
56 S. Ullah, M. A. Assiri, A. G. Al-Sehemi, M. A. Bustam, H. A. Mannan, F. A. Abdulkareem, A. Irfan and S. Saqib, *Greenhouse Gases: Sci. Technol.*, 2019, **9**, 1010–1026.
57 M. Mubashir, Y. F. Yeong and K. K. Lau, *J. Nat. Gas Sci. Eng.*, 2016, **30**, 50–63.
58 Q. Zhang, X. Lian, R. Krishna, S.-Q. Yang and T.-L. Hu, *Sep. Purif. Technol.*, 2023, **304**, 122312.
59 S.-Q. Yang, R. Krishna, L. Zhou, Y.-L. Li, B. Xing, Q. Zhang, F.-Y. Zhang and T.-L. Hu, *Sep. Purif. Technol.*, 2024, **329**, 125167.
60 L. Li, R.-B. Lin, R. Krishna, H. Li, S. Xiang, H. Wu, J. Li, W. Zhou and B. Chen, *Science*, 2018, **362**, 443–446.
61 X. Cui, K. Chen, H. Xing, Q. Yang, R. Krishna, Z. Bao, H. Wu, W. Zhou, X. Dong, Y. Han, B. Li, Q. Ren, M. J. Zaworotko and B. Chen, *Science*, 2016, **353**, 141–144.
62 Z. R. Herm, B. M. Wiers, J. A. Mason, J. M. van Baten, M. R. Hudson, P. Zajdel, C. M. Brown, N. Masciocchi, R. Krishna and J. R. Long, *Science*, 2013, **340**, 960–964.
63 E. D. Bloch, W. L. Queen, R. Krishna, J. M. Zadrozny, C. M. Brown and J. R. Long, *Science*, 2012, **335**, 1606–1610.
64 R. Krishna, *Chem. Soc. Rev.*, 2015, **44**, 2812–2836.
65 R. Krishna, *Chem. Soc. Rev.*, 2012, **41**, 3099–3118.

Electronic Supplementary Information (ESI)

An Ethynyl-Modified Interpenetrated Metal-Organic Framework for Highly Efficient Selective Gas Adsorption

Xueyue Yu,[a] Ziyang Huang,[b] Rajamani Krishna,[C] Xiaolong Luo*[a, b] and Yunling Liu*[a]

[a] State Key Laboratory of Inorganic Synthesis & Preparative Chemistry, Jilin University, Changchun 130012, P. R. China

E-mail: yunling@jlu.edu.cn; Fax: +86 431 85168624

[b] School of Chemistry and Life Science, Advanced Institute of Materials Science, Changchun University of Technology, Changchun, 130012, P. R. China

[C] Van 't Hoff Institute for Molecular Sciences, University of Amsterdam, Science Park 904, 1098 XH Amsterdam, The Netherlands.

E-mail: r.krishna@contact.uva.nl

Calculation procedures of selectivity from IAST

The ideal adsorption solution theory (IAST) was used to predict the binary mixture adsorption from the experimental pure-gas isotherms. The single-component isotherms were fitted using a dual-site Langmuir-Freundlich (DSLF) equation:

$$q = q_{m1} \cdot \frac{b_1 \cdot p^{1/n_1}}{1 + b_1 \cdot p^{1/n_1}} + q_{m2} \cdot \frac{b_2 \cdot p^{1/n_2}}{1 + b_2 \cdot p^{1/n_2}}$$

Here, p is the pressure of the bulk gas at equilibrium with the adsorbed phase (kPa), q is the adsorbed amount per mass of adsorbent (mmol/g), q_{m1} and q_{m2} are the saturation capacities of sites 1 and 2 (mmol/g), b_1 and b_2 are the affinity coefficients of sites 1 and 2 (1/kPa), and n_1 and n_2 represent the deviations from an ideal homogeneous surface.

To investigate the separation of binary mixtures, the adsorption selectivity is defined as follows equation:

$$S = \frac{q_1/q_2}{p_1/p_2}$$

Where q_i and p_i (i=1, 2) are the mole fractions of component 1 and 2 in the adsorbed and bulk phases, respectively. The IAST calculations were carried out for binary mixture containing equimolar gas.

Calculations of the Isosteric Heats of Gas Adsorption (Q_{st}):

A virial-type[30] expression comprising the temperature-independent parameters a_i and b_j was employed to calculate the enthalpies of adsorption for CO_2, CH_4, C_2H_6, C_3H_8, C_2H_4 and C_2H_2 (at 273and 298 K) on compounds. In each case, the data were fitted using the equation:

$$ln^P = ln^N + {}^1/_T \sum_{i-0}^{m} a_i N^i + \sum_{j-0}^{n} b_j N^j$$

Here, P is the pressure expressed in Torr, N is the amount adsorbed in mmol g^{-1}, T is the temperature in K, a_i and b_j are virial coefficients, m, n represent the number of coefficients required to adequately describe the isotherms (m and n were gradually increased until the contribution of extra added a and b coefficients was deemed to be statistically insignificant towards the overall fit, and the average value of the squared deviations from the experimental values was minimized). The values of the virial coefficients a_0 through a_m were then used to calculate the isosteric heat of adsorption using the following expression.

$$Q_{st} = -R \sum_{i-0}^{m} a_i N^i$$

Q_{st} is the coverage-dependent isosteric heat of adsorption and R is the universal gas constant. The heat of gas sorption for compound **1** in this manuscript are determined by using the sorption data measured in the pressure range from 0-1 bar (273 and 298 K for gases), which is fitted by the virial-equation very well.

Transient breakthrough simulations

Transient breakthrough simulations were carried out using the methodology described in earlier publications.[1-5] In these simulations, intra-crystalline diffusion influences are ignored.

The simulations were performed in a fixed bed with the following parameters: adsorber length, L = 0.3 m; cross-sectional area, A = 1 m^2; interstitial gas velocity in the bed, v = 0.1 m s^{-1}; voidage of the packed bed, ε = 0.4; the superficial gas velocity at the inlet to the bed, u_0 = 0.04 m s^{-1}. The volumetric flow rate of the gas mixture at the inlet Q_0 = 40 L s^{-1}. The volume of MOF used in the simulations is $V_{ads} = LA(1-\varepsilon)$ = 0.18 m^3 = 180 L. The total volume of the bed is $V_{bed} = LA$. It is important to note that the volume of adsorbent, V_{ads}, includes the pore volume of the adsorbent material. If ρ is the

framework density, the mass of the adsorbent in the bed is $m_{ads} = (1-\varepsilon)\times(L\ \text{m})\times(A\ \text{m}^2)\times(\rho\ \text{kg m}^{-3})$ kg.

The mixture adsorption equilibrium were determined using the Ideal Adsorbed Solution Theory (IAST) of Myers and Prausnitz;[6] the unary isotherm data fits.

The breakthrough data are presented in terms of the dimensionless concentrations at the exit of the fixed bed, c_i/c_{i0}, as function of the modified time parameter

$$\frac{(Q_0 = \text{flow rate L s}^{-1})\times(\text{time in s})}{(\text{kg MOF packed in tube})} = \frac{Q_0 t}{m_{ads}} = \text{L kg}^{-1}.$$

Notation

L length of packed bed adsorber, m

m_{ads} mass of adsorbent packed in fixed bed, kg

Q_0 volumetric flow rate of gas mixture entering fixed bed, $m^3\ s^{-1}$

u superficial gas velocity in packed bed, $m\ s^{-1}$

v interstitial gas velocity in packed bed, $m\ s^{-1}$

Greek letters

ε voidage of packed bed, dimensionless

ρ framework density, $kg\ m^{-3}$

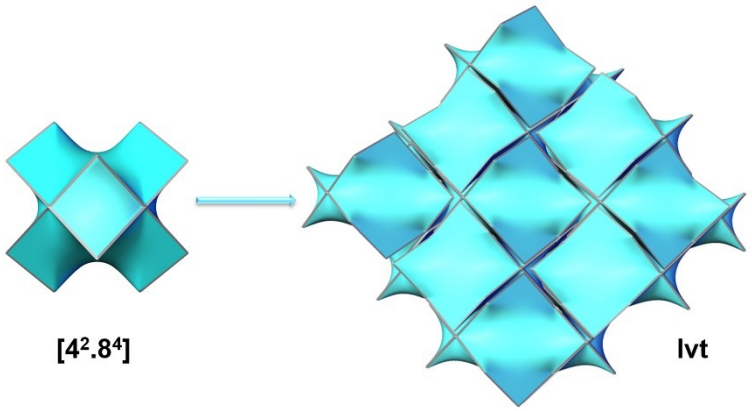

Figure S1. Topological features of compound **1** displayed by tiles and face symbols for blue tile is [$4^2.8^4$].

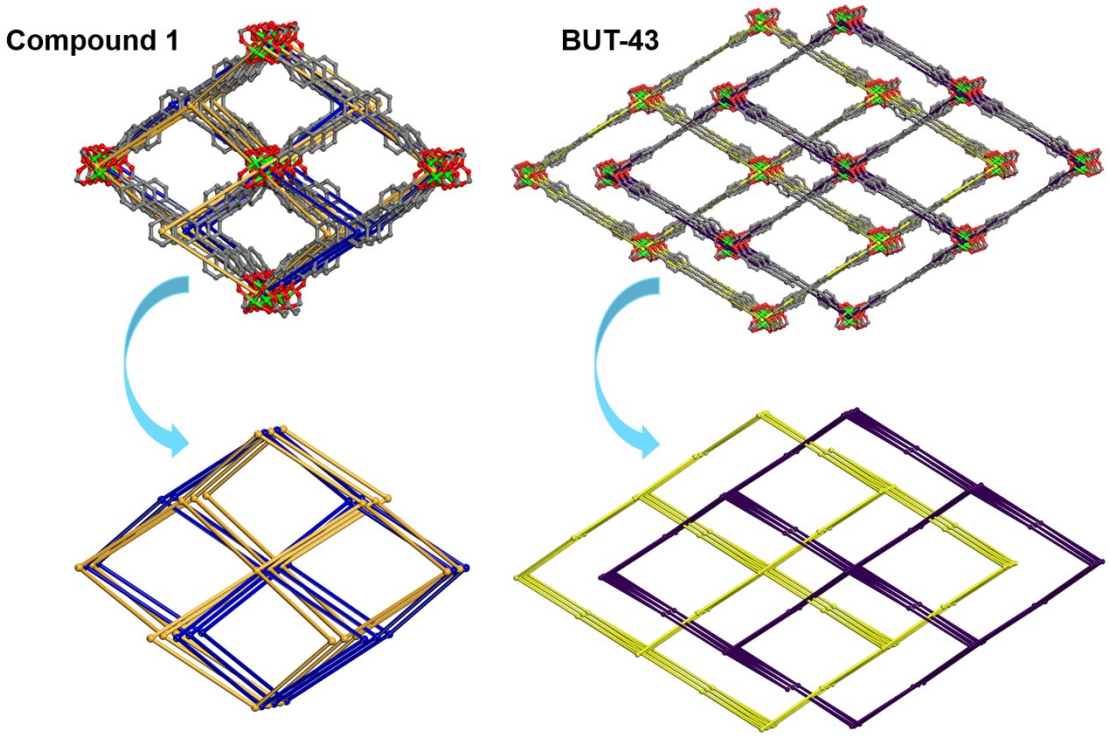

Figure S2. The difference between compound **1** and BUT-43 in the degree of interpenetration.

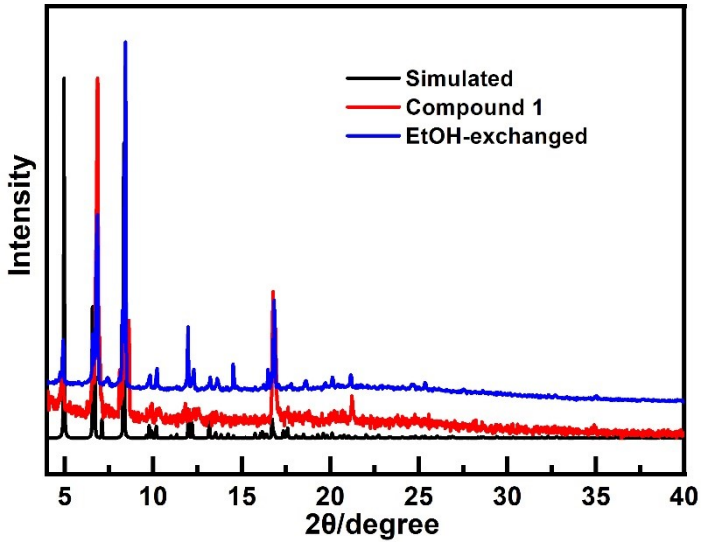

Figure S3. The PXRD patterns of simulated, as-synthesized and EtOH-exchanged.

Figure S4. Single crystal optical images of compound **1**.

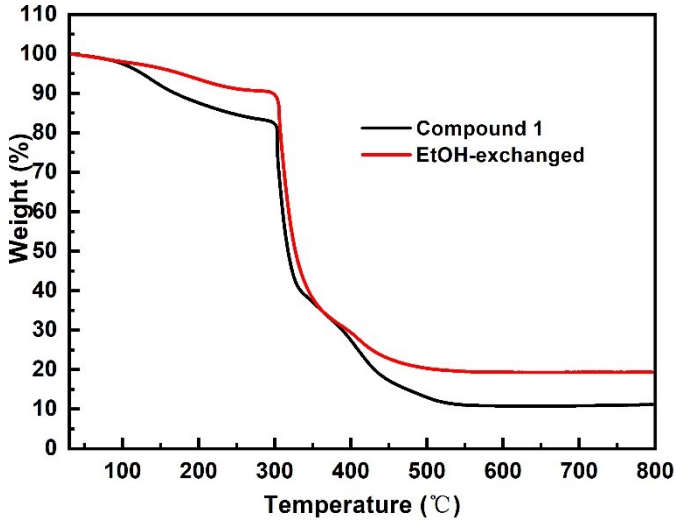

Figure S5. Thermogravimetric analysis curves of as-synthesized and after ethanol exchanged samples for compound **1**.

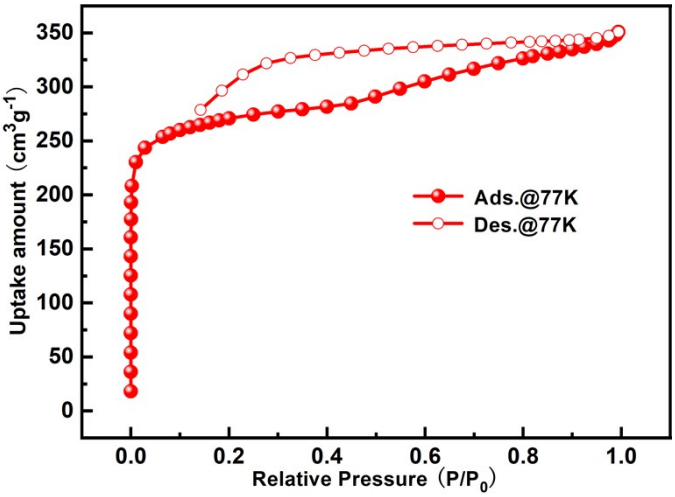

Figure S6. N_2 isotherms for compound **1** at 77 K under 1 atm.

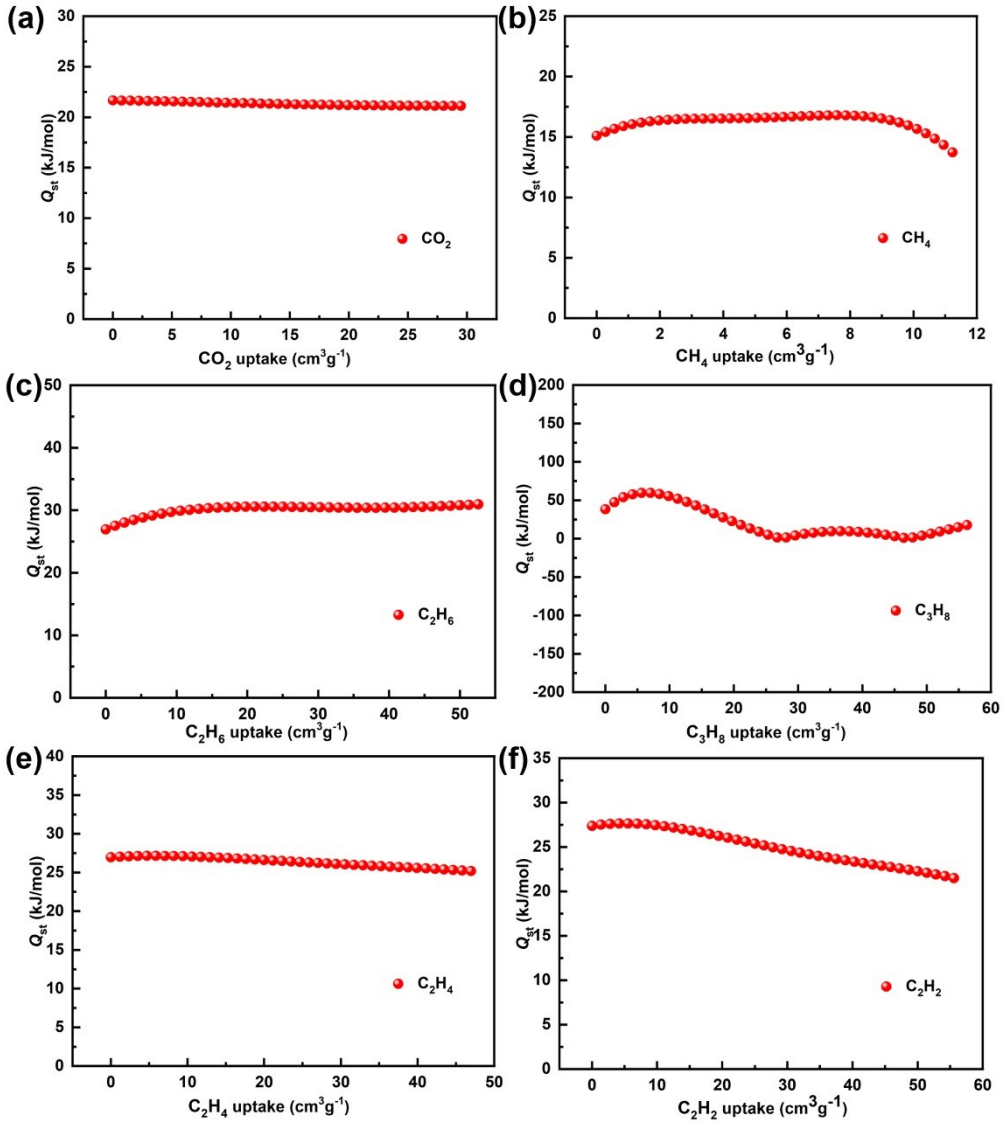

Figure S7. Q_{st} of (a) CO_2; (b) CH_4; (c) C_2H_6; (d) C_3H_8; (e) C_2H_4; (f) C_2H_2 for compound **1**.

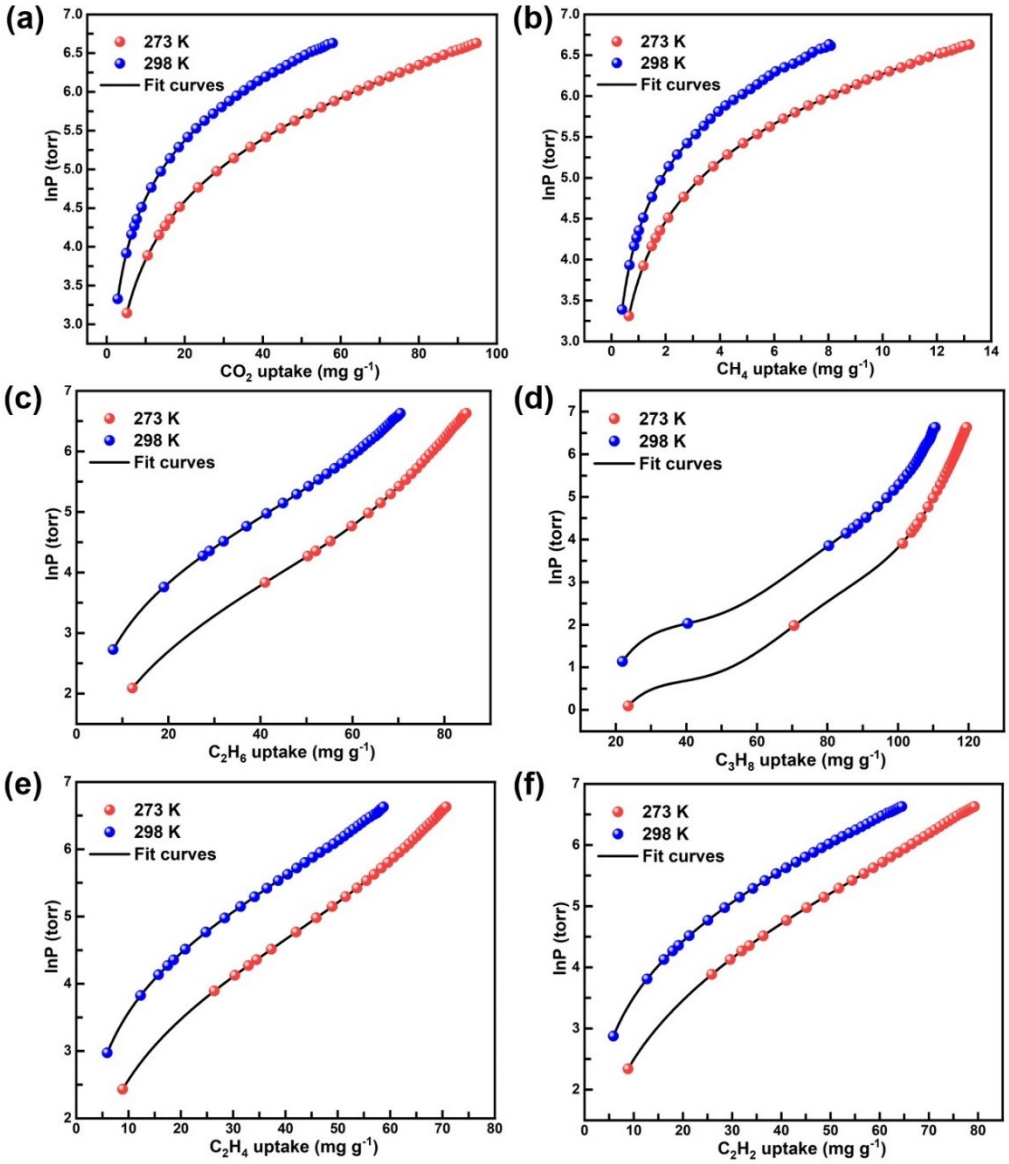

Figure S8. Nonlinear curves fitting of compound **1** for CO_2 (a), CH_4 (b), C_2H_6 (c), C_3H_8 (d), C_2H_4 (e) and C_2H_2 (f) at 273 K and 298 K.

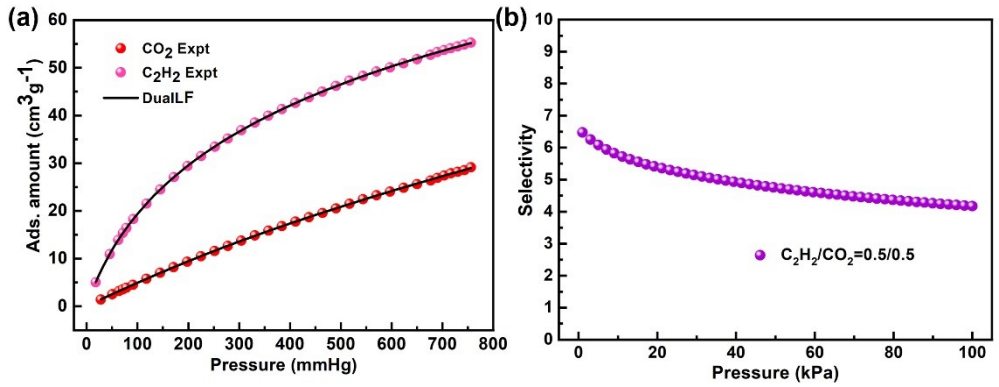

Figure S9. (a) C_2H_2 and CO_2 adsorption isotherms at 298 K along with the DSLF fits; (b) C_2H_2/CO_2 selectivity of compound **1** at 298 K by the IAST method.

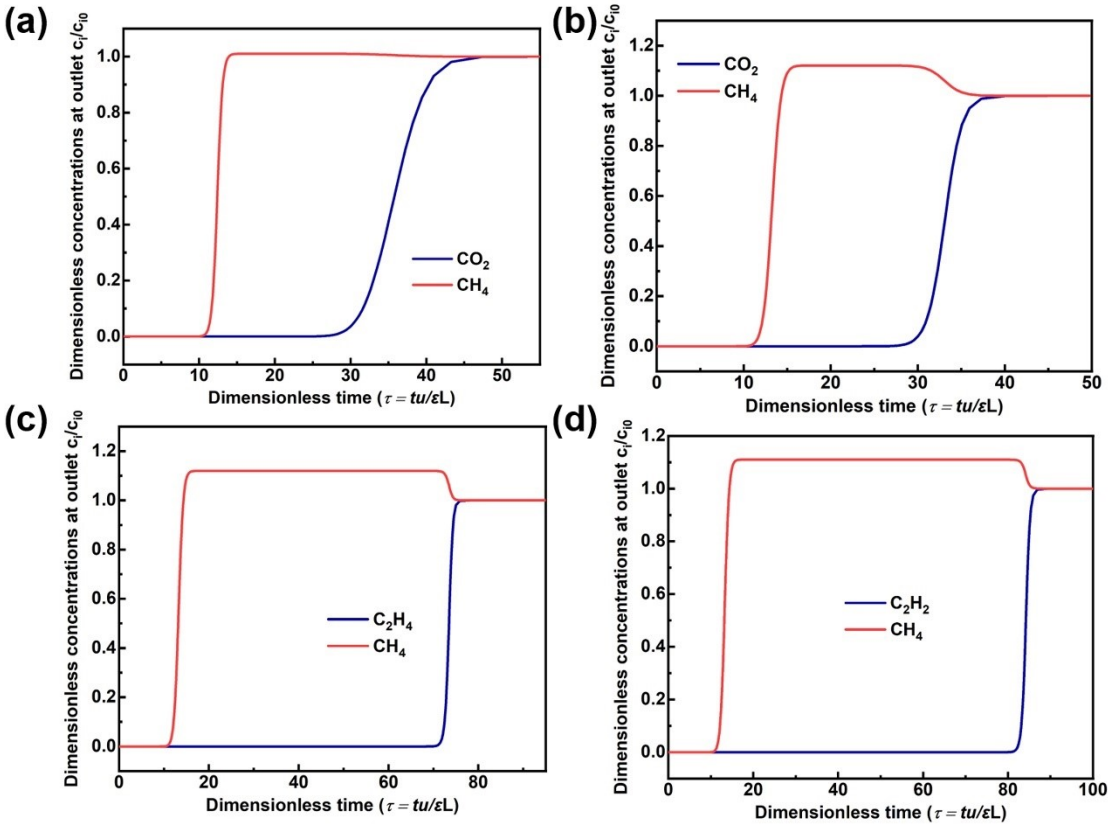

Figure S10. Transient breakthrough simulations for separation of 5/95 and 50/50 (a and b) CO_2/CH_4, 50/50 and 50/50 C_2H_4/CH_4 and C_2H_2/CH_4 (c and d) mixtures containing. The total inlet pressure is 100 kPa. The *y*-axis is the dimensionless concentrations at the exit, normalized with respect to the inlet concentrations.

Table S1. Crystallographic data and structure refinement for compound **1**.

compound	**Compound 1**
Formula	$C_{23}H_{14}CuO_5N$
Formula weight	447.90
Temperature (K)	273(2)
Wavelength (Å)	0.71073
Crystal system	Orthorhombic
Space group	*Cmca*
a (Å)	26.4044(8)
b (Å)	35.6894(11)
c (Å)	17.4068(5)
α (°)	90
β (°)	90
γ (°)	90
Volume (Å^3)	16403.4(9)
Z	16
F(000)	3648
θ range (deg)	2.21 to 23.94
reflns collected/unique	51994 / 7469
R_{int}	0.0563
data/restraints/params	3092 / 73 / 299
Goodness-of-fit on F^2	1.011
R_1, wR_2 [$I>2\sigma(I)$]	0.0489, 0.1452
R_1, wR_2 (all data)	0.0837, 0.1758

Table S2. Selected bond lengths (Å) and angles (°) for compound **1**.

Cu(1)-O(2)	1.957(2)	O(1)-Cu(1)-O(5)	93.10(10)
Cu(1)-O(4)	1.963(2)	O(3)-Cu(1)-O(5)	92.90(10)
Cu(1)-O(1)	1.960(2)	O(2)-Cu(1)-Cu(1)#1	83.76(8)
Cu(1)-O(3)	1.970(2)	O(4)-Cu(1)-Cu(1)#1	86.83(7)
Cu(1)-O(5)	2.127(3)	O(1)-Cu(1)-Cu(1)#1	84.89(8)
O(2)-Cu(1)-O(4)	89.29(10)	O(3)-Cu(1)-Cu(1)#1	81.63(7)
O(2)-Cu(1)-O(1)	168.64(11)	O(5)-Cu(1)-Cu(1)#1	174.18(7)
O(4)-Cu(1)-O(1)	89.57(9)	C(21)-O(1)-Cu(1)	121.7(2)
O(2)-Cu(1)-O(3)	89.55(10)	C(21)#1-O(2)-Cu(1)	123.1(2)
O(4)-Cu(1)-O(3)	168.46(10)	C(1)#1-O(3)-Cu(1)	125.8(2)
O(1)-Cu(1)-O(3)	89.31(10)	C(1)-O(4)-Cu(1)	120.4(2)
O(2)-Cu(1)-O(5)	98.25(10)	C(22A)-O(5)-Cu(1)	121.7(6)
O(4)-Cu(1)-O(5)	98.63(10)	C(22B)-O(5)-Cu(1)	120.8(4)

Symmetry transformations used to generate equivalent atoms: #1 -x+y,-x+1,z #2 -y+1,x-y+1,z #3 y,-x+y,-z+1 #4 y,-x+y,z-1/2 #5 x,y,-z+1/2 #6 x-y,x,-z+1 #7 x,y,-z+3/2

Table S3. Comparison of the crystal data for compound **1** and BUT-43

Compound	Compound **1**	BUT-43
Formula	$C_{23}H_{14}CuO_5N$	$C_{42}H_{22}Cu_2O_{10}$
Crystal system	Orthorhombic	Monoclinic
Space group	*Cmca*	*C*2/*c*
a (Å)	26.4044(8)	42.7195(15)
b (Å)	35.6894(11)	23.6272(18)
c (Å)	17.4068(5)	21.5936(9)
α (°)	90	90
β (°)	90	120.317
γ (°)	90	30
V (Å³)	16403.4(9)	18814.8(19)

Table S4. C_3H_8/CH_4 selectivity performance comparison of some previous reported MOFs.

Compound	**Selectivity (0.5:0.5)**	**Ref.**
MIL-142A	1300	7
LSHU01’	912.6	8
ZUL-C2	632	9
BSF-1	353	10
JLU-MOF66	308.4	11
Cu-IPA	296	12
JLU-MOF67	287.1	11
JLU-MOF51	220	13
Compound **1**	204.7	This work
CTGU-15	170.7	14
FJI-H21	145.2	15
NUM-18a	109	16
ANPC-1-800	110.4	17
Zr-OBBA	105.6	18
Zr-SDBA	97.5	18
FIR-7a-ht	78.8	19
FJI-C1	78.7	20
UPC-21	67	21
JLU-Liu45	42.7	18

Table S5. C_2H_2/CO_2 selectivity performance comparison of some previous reported MOFs.

Compound	Selectivity (0.5:0.5)	Ref.
ZJU-74a	36.5	22
SNNU-65-Cu-Ga	18.7	23
BUT-70A	14.8	24
SNNU-65-Cu-Sc	13.5	23
BUT-70B	11.2	24
ZJUT-2a	10	25
CPM-107	5.7	26
Compound **1**	4.2	This work
UTSA-222	4.0	27
$Cu(BDC\text{-}Br)(H_2O)_{0.5}(DMF)_{2.5}$	3.9	28
ZJNU-100	3.8	29
MFM-127	3.7	30
UPC-112	2.8	31
FJU-36	2.8	32

Table S6. The refined parameters for the DSLF equations fit for the pure isotherms of CO_2, CH_4, C_2H_6, C_3H_8, C_2H_4 and C_2H_2 for compound **1** at 298 K.

	q_{m1}	b_1	n_1	q_{m2}	b_2	n_2	R^2
CO_2	166.64366	0.0025	0.9522	1.00888	6.08931E-4	2.21422	0.99993
CH_4	0.07206	0.1284	1.36881	56.16216	0.00225	1.01347	0.99967
C_2H_6	152.77597	6.91914E-15	5.78602	62.15591	0.05249	0.98972	0.99999
C_3H_8	14.9987	0.06968	0.96147	43.47711	0.80333	1.02696	0.99998
C_2H_4	55.60565	0.03473	0.97379	15.65395	0.00575	0.93268	0.99997
C_2H_2	85.37359	0.00909	0.88842	30.04471	0.05592	0.97088	0.99998

Table S7. The fitting parameters of the virial model with the isotherms at 273 and 298K for CO_2, CH_4, C_2H_6, C_3H_8, C_2H_4 and C_2H_2 for compound **1**.

	a_0	a_1	a_2	a_3	b_0	b_1	b_2	R^2
CO_2	-2605.14006	1.50895	0.24141	-0.01282	11.02857	0.00313	4.7993E-4	0.99999
CH_4	-1815.58629	-148.47707	47.51895	-6.38126	10.39606	0.55578	-0.17381	0.99994
C_2H_6	-3240.78779	-55.26564	2.49881	-0.05038	11.44351	0.19071	-0.00755	0.99998
C_3H_8	-3323.6	-21.07502	0.38401	-0.06539	4.22101	0.47945	-0.00874	0.99985
C_2H_4	-3244.28023	-7.90039	0.8914	-0.02651	11.97116	0.04476	-0.00284	0.99998
C_2H_2	-3291.98574	-14.22141	1.65403	-0.03152	11.99716	0.07767	-0.00625	0.99999

REFERENCES

1. R. Krishna, *Microporous Mesoporous Mater.*, 2014, **185**, 30-50.
2. R. Krishna, *RSC Advances*, 2015, **5**, 52269-52295.
3. R. Krishna, *RSC Advances*, 2017, **7**, 35724-35737.
4. R. Krishna, *Sep. Purif. Technol.*, 2018, **194**, 281-300.
5. R. Krishna, *ACS Omega*, 2020, **5**, 16987-17004.
6. A. L. Myers and J. M. Prausnitz, *A.I.Ch.E.J.* **1965**, *11*, 121-130.
7. Y. Yuan, H. Wu, Y. Xu, D. Lv, S. Tu, Y. Wu, Z. Li and Q. Xia, *Chem. Eng. J.*, 2020, **395**, 125057.
8. D. Geng, X. Han, Y. Bi, Y. Qin, Q. Li, L. Huang, K. Zhou, L. Song and Z. Zheng, *Chem. Sci.*, 2018, **9**, 8535.
9. J. Zhou, T. Ke, F. Steinke, N. Stock, Z. Zhang, Z. Bao, X. He, Q. Ren and Q. Yang, *J. Am. Chem. Soc.*, 2022, **144**, 14322.
10. Y. Zhang, L. Yang, L. Wang, S. Duttwyler and H. Xing, *Angew. Chem. Int. Ed.*, 2019, **58**, 8145.
11. L. Kan, G. Li and Y. Liu, *ACS Appl. Mater. Interfaces*, 2020, **12**, 18642.
12. D. Lin, S. Tu, L. Yu, Y. Yuan, Y. Wu, X. Zhou, Z. Li and Q. Xia, *Ind. Eng. Chem. Res.*, 2023, **62**, 5252.
13. D. Wang, J. Zhang, G. Li, J. Yuan, J. Li, Q. Huo and Y. Liu, *ACS Appl. Mater. Interfaces*, 2018, **10**, 31233.
14. D. Lv, Z. Liu, F. Xu, H. Wu, W. Yuan, J. Yan, H. Xi, X. Chen and Q. Xia, *Sep. Purif. Technol.*, 2021, **266**, 118198.
15. P. Huang, C. Chen, M. Wu, F. Jiang and M. Hong, *Dalton Trans.*, 2019, **48**, 5527.
16. Q. Zhang, X. Lian, R. Krishna, S.-Q. Yang and T.-L. Hu, *Sep. Purif. Technol.*, 2023, **304**, 122312.
17. P. Zhang, X. Wen, L. Wang, Y. Zhong, Y. Su, Y. Zhang, J. Wang, J. Yang, Z. Zeng and S. Deng, *Chem. Eng. J.*, 2020, **381**, 122731.
18. J. Gu, X. Sun, L. Kan, J. Qiao, G. Li and Y. Liu, *ACS Appl. Mater. Interfaces*, 2021, **13**, 41680.

19. J. E. Bachman, M. T. Kapelewski, D. A. Reed, M. I. Gonzalez and J. R. Long, *J. Am. Chem. Soc.*, 2017, **139**, 15363.
20. D. A. Reed, B. K. Keitz, J. Oktawiec, J. A. Mason, T. Runčevski, D. J. Xiao, L. E. Darago, V. Crocellà, S. Bordiga and J. R. Long, *Nature*, 2017, **550**, 96.
21. T. Grancha, M. Mon, J. Ferrando-Soria, J. Gascon, B. Seoane, E. V. Ramos-Fernandez, D. Armentano and E. Pardo, *J. Mater. Chem. A.*, 2017, **5**, 11032.
22. J. Pei, K. Shao, J.-X. Wang, H.-M. Wen, Y. Yang, Y. Cui, R. Krishna, B. Li and G. Qian, *Adv. Mater.*, 2020, **32**, 1908275.
23. J.-W. Zhang, M.-C. Hu, S.-N. Li, Y.-C. Jiang, P. Qu and Q.-G. Zhai, *Chem. Commun.*, 2018, **54**, 2012.
24. Z.-J. Guo, J. Yu, Y.-Z. Zhang, J. Zhang, Y. Chen, Y. Wu, L.-H. Xie and J.-R. Li, *Inorg. Chem.*, 2017, **56**, 2188.
25. H.-M. Wen, C. Liao, L. Li, L. Yang, J. Wang, L. Huang, B. Li, B. Chen and J. Hu, *Chem. Commun.*, 2019, **55**, 11354.
26. H. Yang, T. X. Trieu, X. Zhao, Y. Wang, Y. Wang, P. Feng and X. Bu, *Angew. Chem. Int. Ed.*, 2019, **58**, 11757.
27. J.-x. Ma, J. Guo, H. Wang, B. Li, T. Yang and B. Chen, *Inorg. Chem.*, 2017, **56**, 7145.
28. H. Cui, Y. Ye, H. Arman, Z. Li, A. Alsalme, R.-B. Lin and B. Chen, *Cryst. Growth Des.*, 2019, **19**, 5829.
29. Y. Wang, M. He, X. Gao, X. Wang, G. Xu, Z. Zhang and Y. He, *Inorganic Chemistry Frontiers*, 2019, **6**, 263.
30. J. D. Humby, O. Benson, G. L. Smith, S. P. Argent, I. da Silva, Y. Cheng, S. Rudić, P. Manuel, M. D. Frogley, G. Cinque, L. K. Saunders, I. J. Vitórica-Yrezábal, G. F. S. Whitehead, T. L. Easun, W. Lewis, A. J. Blake, A. J. Ramirez-Cuesta, S. Yang and M. Schröder, *Chemical Science*, 2019, **10**, 1098.
31. W. Fan, X. Wang, X. Liu, B. Xu, X. Zhang, W. Wang, X. Wang, Y. Wang, F. Dai, D. Yuan and D. Sun, *ACS Sustainable Chemistry & Engineering*, 2019, **7**, 2134.
32. L. Liu, Z. Yao, Y. Ye, L. Chen, Q. Lin, Y. Yang, Z. Zhang and S. Xiang, *Inorg. Chem.*, 2018, **57**, 12961.